

Interface Engineering in BNNS@Ti₃C₂ Intercalation Structure for Enhanced Electrocatalytic Hydrogen Evolution

Zizheng Ai,^[a] Bin Chang,^[a] Chengwei Xu,^[b] Baibiao Huang,^[a] Yongzhong Wu,^[a]
Xiaopeng Hao,^[a] Yongliang shao*^[a]

[a] State Key Lab of Crystal Materials, Shandong University, Jinan 250100, P. R. of
China;

[b] Department of Laboratory Medicine, The Second Hospital of Shandong University,
247 Beiyuan Dajie, Jinan, 250033, P.R. China

Email: ylshao@sdu.edu.cn

S1 Morphology of Ti₃C₂

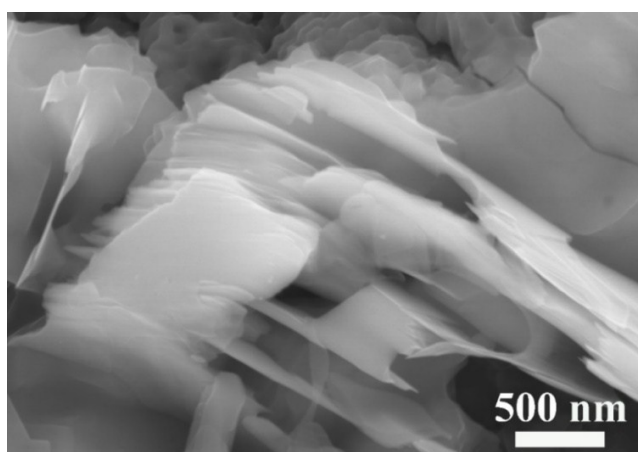


Fig. S1. SEM image of Ti₃C₂

Fig. S1 shows that Ti₃C₂ presents layer structure after HF etching treatment.

S2 AFM image and height profile of BNNS

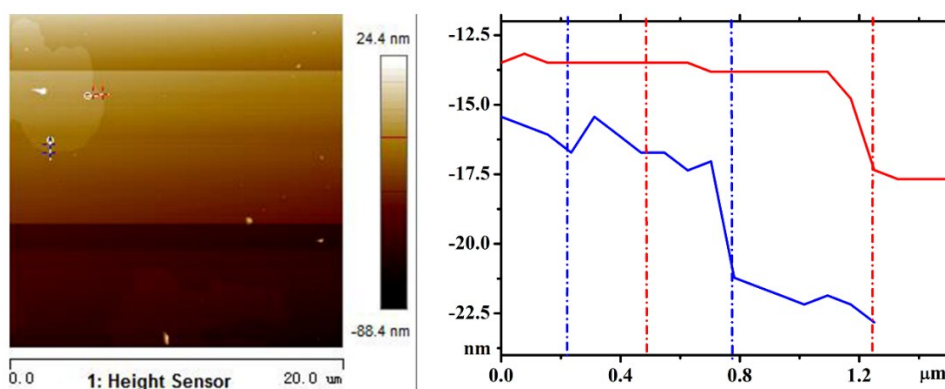


Fig. S2. AFM image and the corresponding height profile (right) of flat BNNS.

It can be seen that BNNS possesses the thickness of about 4 nm through effective exfoliation process of NaOH.

S3 SEM image of BNNS

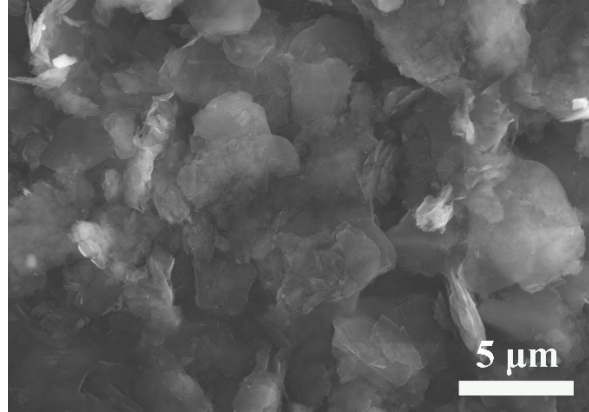


Fig. S3. SEM image of BNNS

In **Fig. S3**, after NaOH treatment, bulk h-BN is exfoliated to few separated layers successfully.

S4 SEM image of Ti_3C_2 after the ball-milling treatment

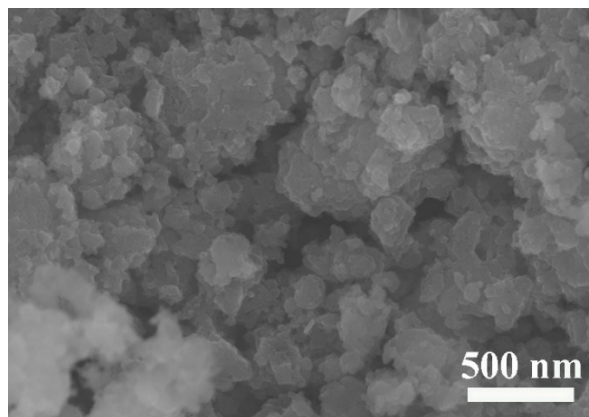


Fig. S4. SEM image of Ti_3C_2 after the ball-milling treatment.

As shown in **Fig. S4**, the construction of Ti_3C_2 is destroyed and becomes broken pieces via ball-milling process.

S5 SEM images of BNNS@ Ti_3C_2 with different compound ratios

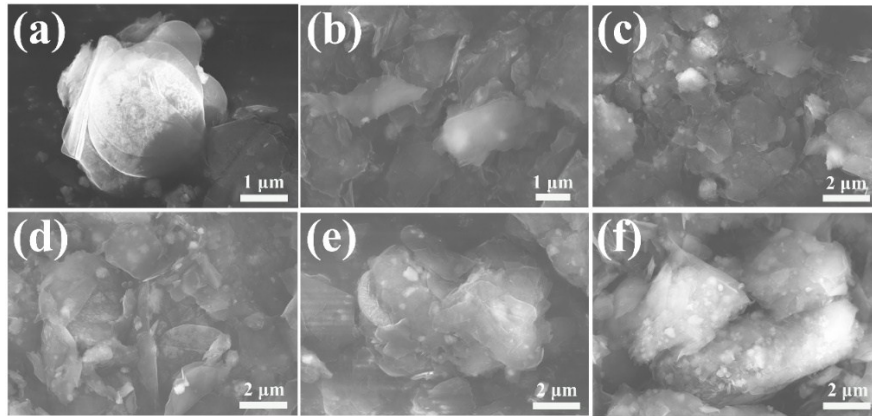


Fig. S5. SEM images of BNNS@Ti₃C₂ with different compound ratios of Ti₃C₂. (a) BT0, (b) BT0.01, (c) BT0.03, (d) BT0.05, (e) BT0.1, (f) BT0.15.

From **Fig. S5**, Ti₃C₂ breaks to pieces and gradually get into the layers of BNNS.

S6 TEM-HRTEM images of BNNS.

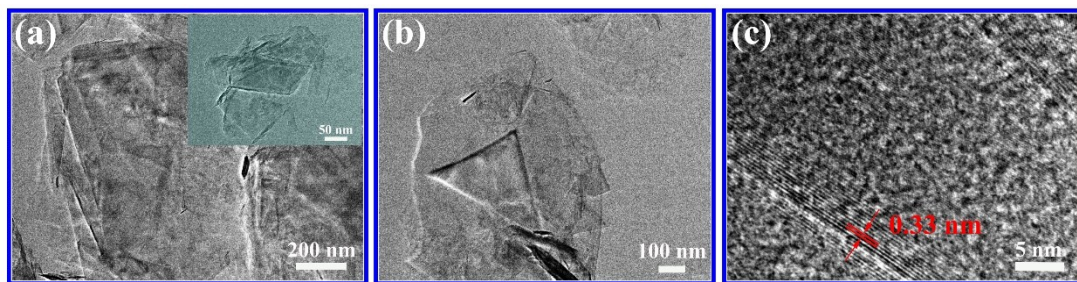


Fig. S6. TEM-HRTEM images of (a-c) BNNS under different magnification.

It can be seen that the exfoliated BNNS aggregate irregularly and crumpled sheets overlap with each other. HRTEM image of BNNS reveals the inter-planar d-spacing of ≈ 0.33 nm corresponding to the (002) plane of h-BN (JCPDS No. 45-0893). Due to the vulnerable stability to electron beam irradiation at 200 kV, the monolayer BNNS can't be presented clearly.

S7 XRD patterns of bulk h-BN and Ti₃C₂.

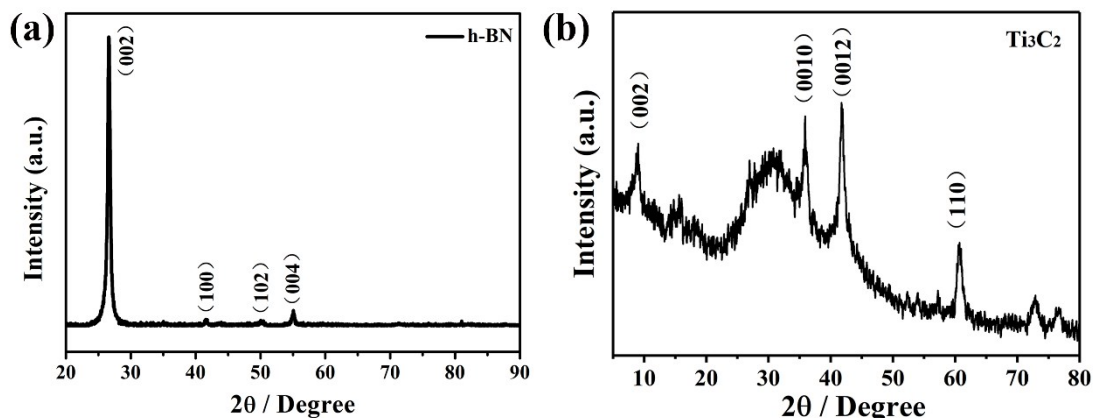


Fig. S7. XRD patterns of bulk h-BN and Ti_3C_2 .

S8 XRD pattern contrast of $\text{BNNS}@ \text{Ti}_3\text{C}_2$ with different compound ratios of Ti_3C_2

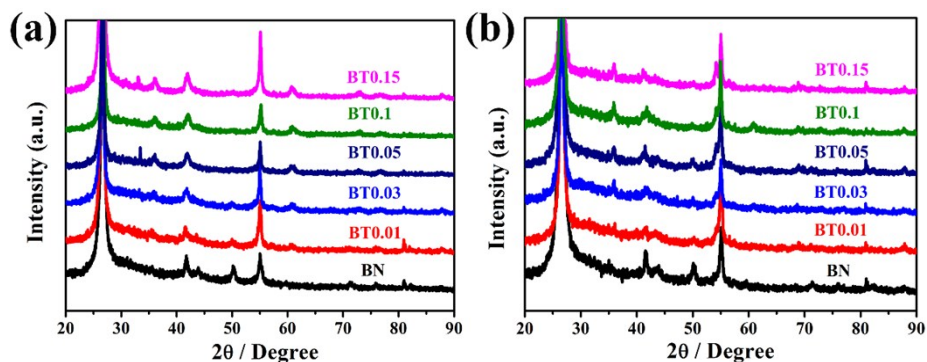


Fig. S8. XRD pattern contrast of $\text{BNNS}@ \text{Ti}_3\text{C}_2$ with different compound ratios of Ti_3C_2 . (a) Before calcination, (b) After calcination.

It can be seen evidently in **Fig. S8** that XRD patterns only have both peaks of h-BN and Ti_3C_2 before calcination and the (102) peak of h-BN fades away as the compound ratio increases, which means that the ball-milling process is a physical mixing experience. After calcination, the (110) peak of Ti_3C_2 disappears and a new peak belonged to $(\text{BN})_{0.33}\text{C}_{0.67}$ appears, whose intensity increasing with the increase of compound ratio.

S9 Raman spectrum of Ti_3C_2

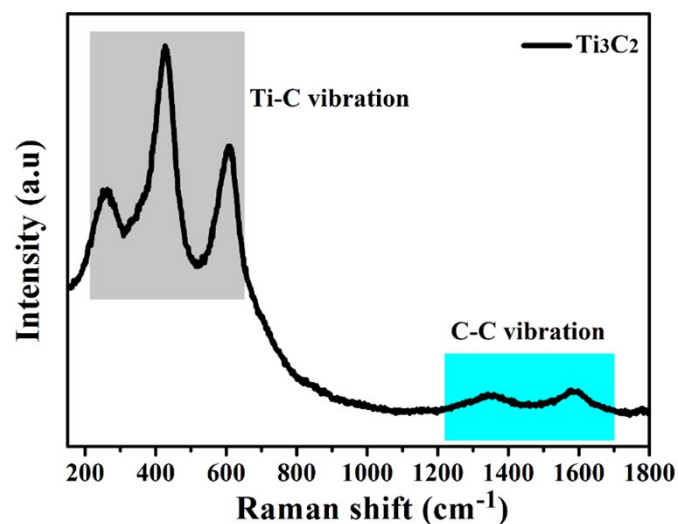


Fig. S9. Raman spectrum of Ti_3C_2 .

Fig. S9 shows that Ti_3C_2 displays three peaks at 260, 420, and 605 cm^{-1} of Ti-C vibration. In addition, there are weak peaks at 1320 and 1590 cm^{-1} . These peaks are associated with the A_{1g} and E_{2g} vibrational modes of graphite, which indicates the presence of some unreacted carbon.

S10 Full XPS spectrum of the BT0.05 sample

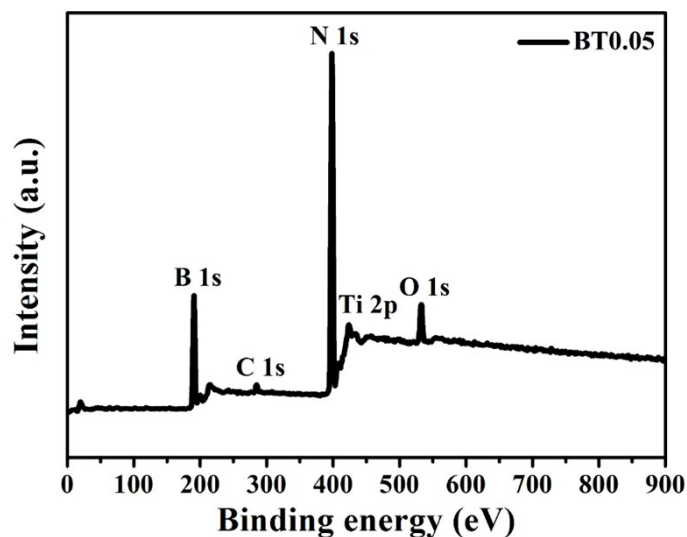


Fig. S10. XPS survey spectrum of the BT0.05 sample.

S11 The LSV curve of bulk h-BN

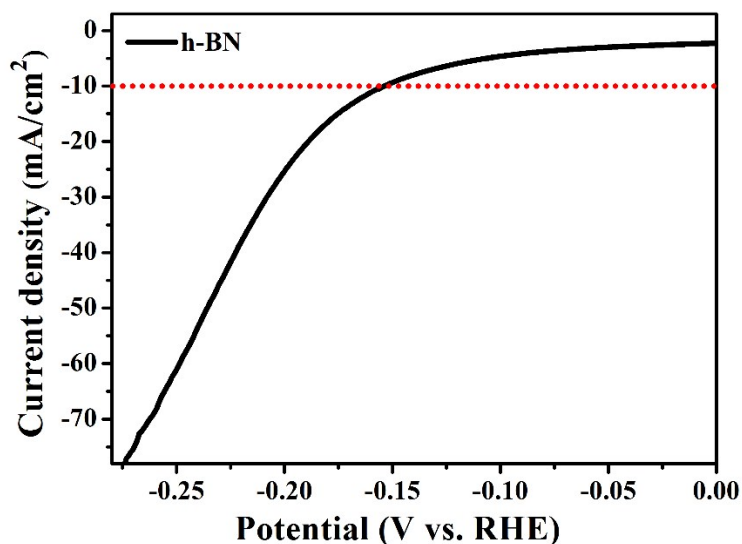


Fig. S11. The LSV curve of bulk h-BN.

Fig. S11 shows that the bulk h-BN electrode has large onset potential (-126 mV) and high overpotential (-157 mV at the current density of $10 \text{ mA}\cdot\text{cm}^{-2}$).

Table S1. Comparison of HER performance of BNNS@Ti₃C₂ electrocatalyst and other non-noble metal-based electrocatalysts.

Electrocatalyst	Onset overpotential (mV)	Overpotential at $10 \text{ mA}\cdot\text{cm}^{-2}$	Tafel slope ($\text{mV}\cdot\text{dec}^{-1}$)	(Ref.)
Ti ₂ CT _x	-75	-170	100	1
Mo ₂ CT _x	-131	-283	N/A	2
MoP	-50	-130	48	3
N-MoSe ₂ /VG	-45	-98	49	4
MoN	-100	-232	90	5
MoSe ₂ /NiSe ₂	-20	-69	42	6
Ni ₂ P	-43	-110	N/A	7
Ni ₃ (VO ₄) ₂	N/A	-90	50	8
BNNS@Ti₃C₂	-23	-52	39	This work

S12 Tafel plots of BNNS@Ti₃C₂ with different compound ratios under different calcination temperatures

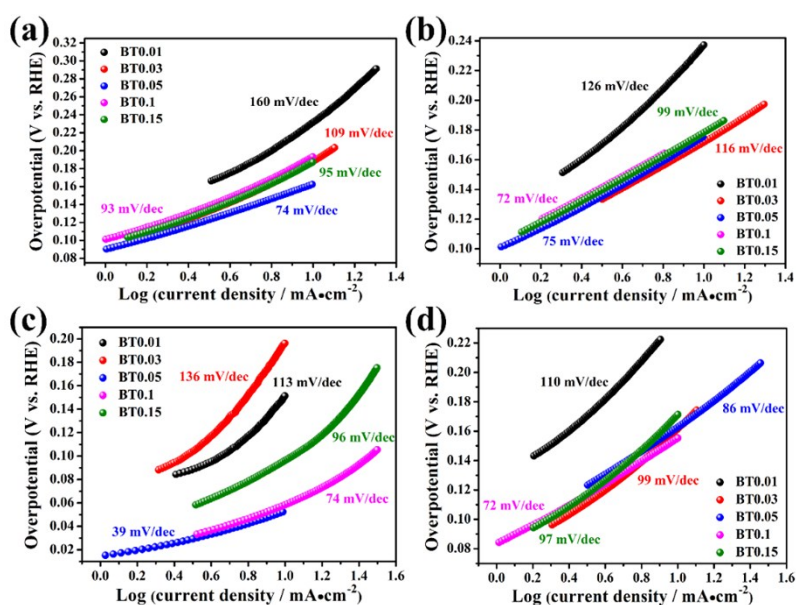


Fig. S12. Tafel plots of the BT0.01, BT0.03, BT0.05, BT0.1 and BT0.15 with different calcination temperatures. (a) 700 °C, (b) 750 °C, (c) 850 °C, (d) 950 °C.

As shown in **Fig. S12**, the smallest Tafel slope can be obtained through tuning the compound ratios.

S13 SEM images of BT0.05 after 20 h stability test

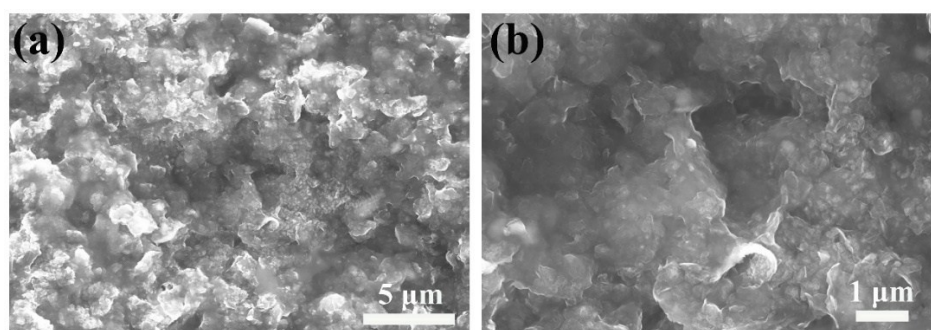


Fig. S13. SEM images of BT0.05 after 20 h stability test.

We can see in **Fig. S13** that the morphology of BT0.05 can keep well after 20 h stability test.

S14 XRD pattern of BT0.05 after 20 h stability test

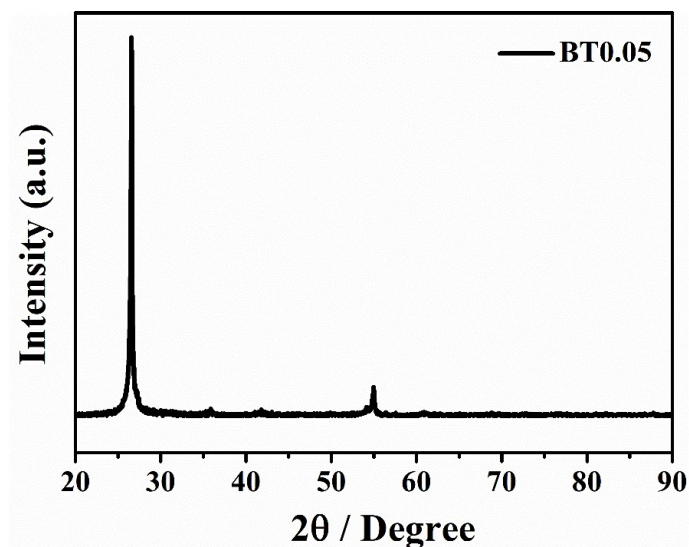


Fig. S14. XRD pattern of BT0.05 after 20 h stability test.

Fig. S14 shows that the crystal structure of BT0.05 can be preserved well after 20 h stability test.

S15 High-resolution XPS spectra of BT0.05 after 20 h stability test

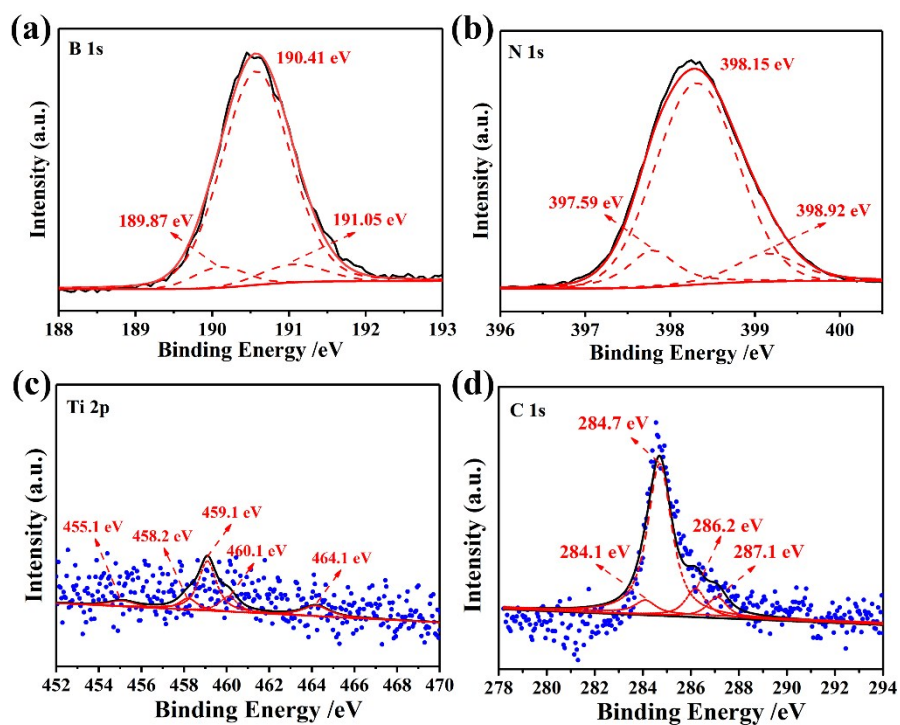


Fig. S15. High-resolution XPS spectra of the BT0.05 after 20 h stability test: (a) B 1s

states, (b) N 1s states, (c) Ti 2p states, (d) C 1s states.

Table S2: Fitting results for equivalent circuits of different samples

Samples	R_s (Ω)	R_{ct} (Ω)
BNNS	4.27	1134
BT0.05	2.76	463

S16 The schematic structural model of BNNS.

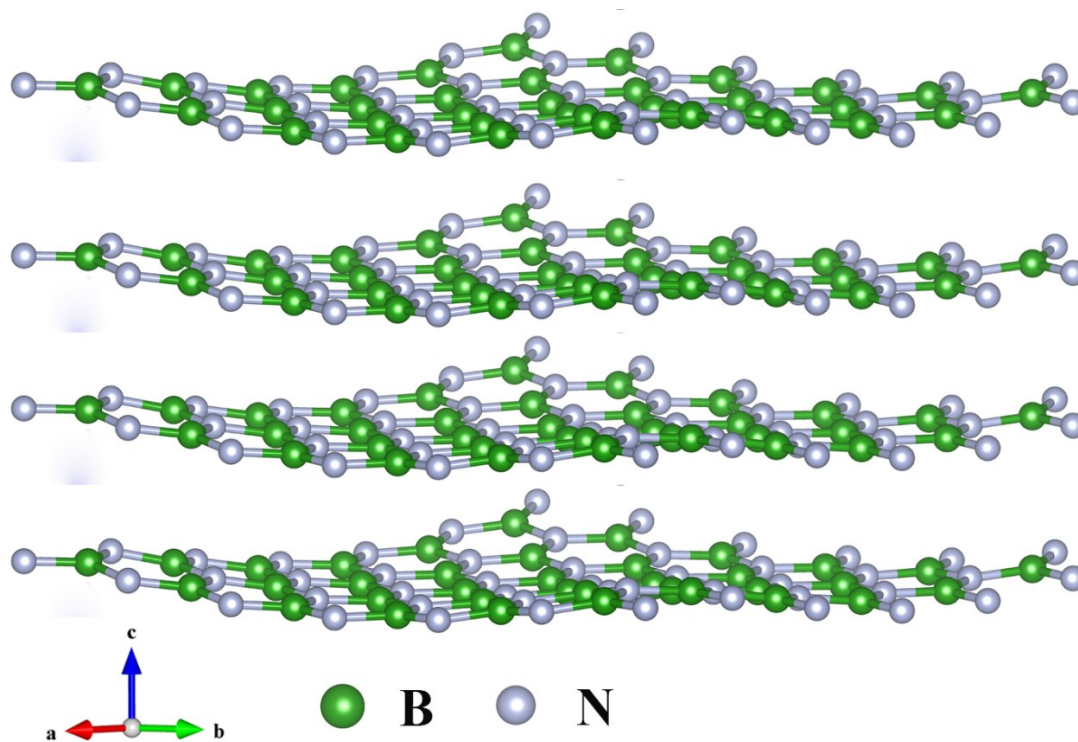


Fig. S16. The structural model for BNNS.

S17 Density of states of BNNS.

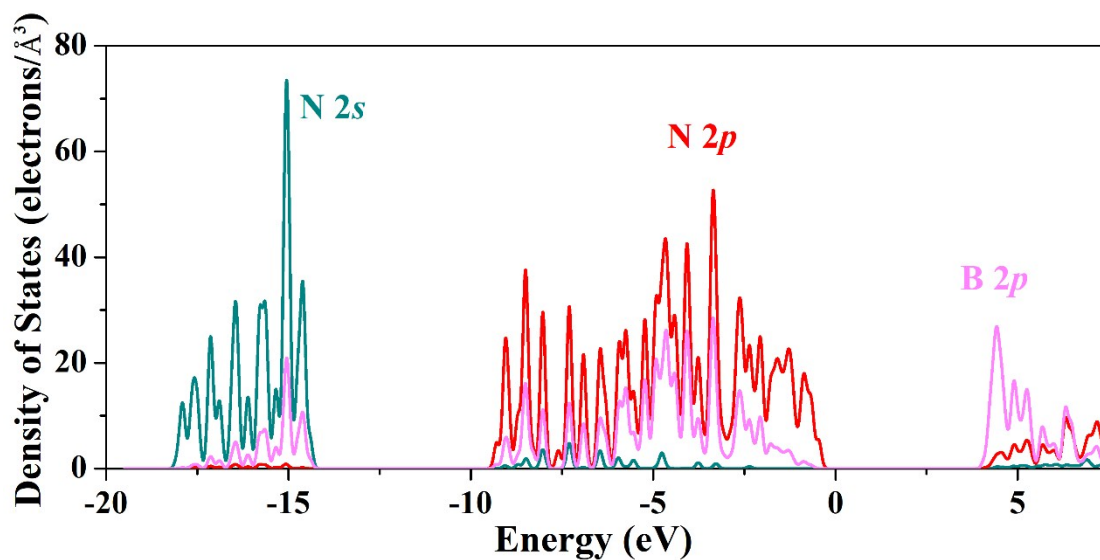


Fig. S17. Density of states of BNNS.

S18 Density of states of BT0.05.

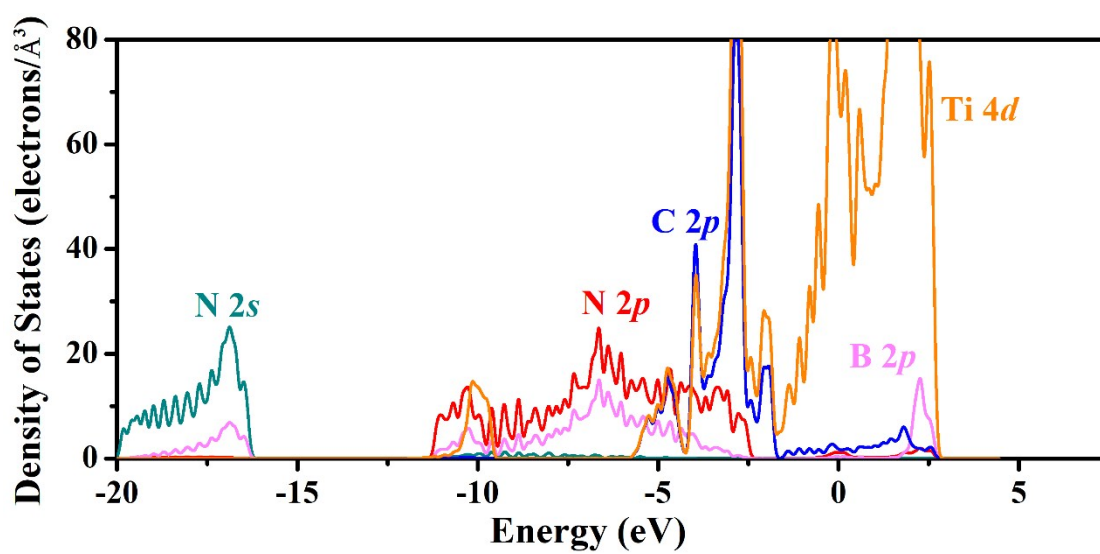


Fig. S18. Density of states of BT0.05.

S19 UV-vis absorption spectra of BNNS and BT0.05.

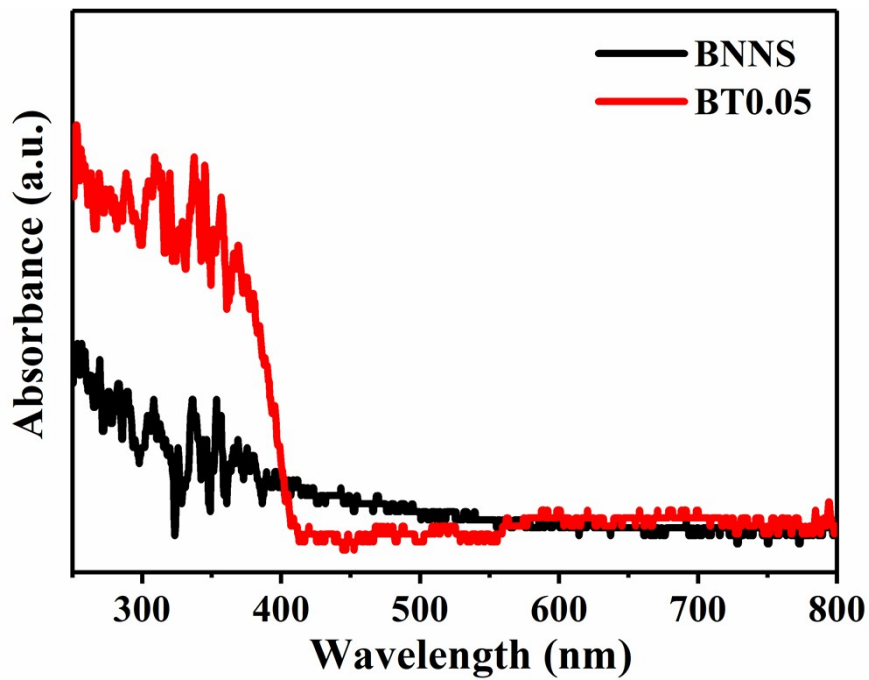


Fig. S19. UV–vis absorption spectra of BNNS and BT0.05.

S20 N₂ adsorption–desorption isotherms of h-BN, BNNS and BT0.05.

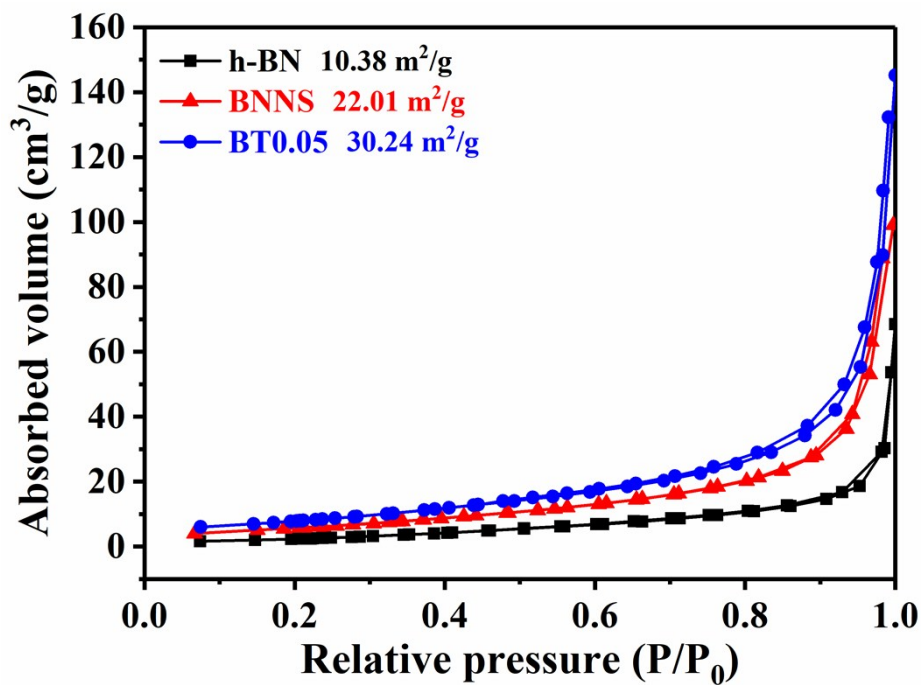


Fig. S20. N₂ adsorption–desorption isotherms of h-BN, BNNS and BT0.05.

References

- [1] S. Li, P. Tuo, J. Xie, X. Zhang, J. Xu, J. Bao, B. Pan, Y. Xie, *Nano Energy*. 2018, **47**, 512-518.
- [2] Z.W. Seh, K.D. Fredrickson, B. Anasori, J. Kibsgaard, A.L. Strickler, M.R. Lukatskaya, Y. Gogotsi, T.F. Jaramillo, A. Vojvodic, *ACS Energy Lett.* 2016, **1**, 589-594.
- [3] P. Xiao, M. Alam, L. Thia, X. M. Ge, R. J. Lim, J. Y. Wang, K. H. Lim, X. Wang, *Energy Environ. Sci.* 2014, **7**, 2624-2629.
- [4] S. Deng, Y. Zhong, Y. Zeng, Y. Wang, Z. Yao, F. Yang, S. Lin, X. Wang, X. Lu, X. Xia, J. Tu, *Adv, Mater.* 2017, **29**, 1700748.
- [5] J. Xie, S. Li, X. Zhang, J. Zhang, R. Wang, H. Zhang, B. Pan, Y. Xie, *Chem. Sci.* 2014, **5**, 4615.
- [6] L. Zhang, T. Wang, L. Sun, Y. J. Sun, T. W. Hu, K. W. Xu, F. Ma, *J. Mater. Chem. A* 2017, **5**, 19752-19759.
- [7] E. J. Popczun, J. R. McKone, C. G. Read, A. J. Biech, A. M. Wiltrout, N. S. Lewis, R. E. Schaak, *J. Am. Chem. Soc.* 2013, **135**, 9267-9270.
- [8] B. Chang, G. Zhao, Y. L. Shao, L. Zhang, B. B. Huang, Y. Z. Wu, X. P. Hao, *J. Mater. Chem. A* 2017, **5**, 18038-18043.